Structure and Magnetic Properties of $Eu_2CaCu_2O_6$

Qiang Xu,*,† Tomasz Klimczuk,‡,§ Jacob Jansen,† Robert J. Cava,‡ and Henny W. Zandbergen†

National Centre for HREM, Kavli Institute of Nanoscience, Delft University of Technology, 2628 CJ Lorentzweg 1, Delft, The Netherlands, Department of Chemistry, Princeton University, Princeton New Jersey 08540, and Faculty of Applied Physics and Mathematics, Gdansk University of Technology, Narutowicza 11/12, 80-952 Gdansk, Poland

Received March 27, 2006. Revised Manuscript Received July 3, 2006

A new type of cuprate, $Eu_2CaCu_2O_6$, has been prepared by high-pressure synthesis. The structure has been determined by high-resolution electron microscopy (HREM) and electron diffraction. A starting structure model was constructed using through-focus exit waves reconstructed from a series of HREM images. The exact structure was determined by refinement using electron diffraction single-crystal data and was confirmed by X-ray Rietveld analysis. The structure consists of CuO_3 planes, containing CuO_4 squares that form separated Cu_2O_6 units, thus giving a zero-dimensional structural character. Magnetic measurements indicate antiferromagnetic behavior with magnetic frustration.

Introduction:

The discovery of high-Tc superconductivity[1] has led to intensive research on cuprate materials. Many different Cu−O structures were found, e.g., chains, zigzag chains, ladders, and planes, depending on the assembling of the CuO_x units. Cu^{2+} ions can have elongated octahedral, square pyramidal, or square coordination. In this geometry, the hole in the 3d shell of the Cu^{2+} ions is orbitally nondegenerate, forming essentially an ideal $S = {}^1/_2$ spin system. The interactions between these spins give cuprates versatile interesting properties.[2−6] The high-Tc cuprates consist of 2-D CuO_2 planes with corner-sharing CuO_6 octahedra, CuO_5 square pyramids, or CuO_4 squares.[7−9] Among the cuprates based on planes of copper and oxygen, four types of planar arrangements have been previously found. These are CuO_2 planes, made from corner sharing of CuO_4 squares,[7−9] and Cu_2O_3 (in $SrCu_2O_3$),[3,5] Cu_3O_4 (in $BaCu_3O_4Cl_2$),[10] and Cu_3O_5 (in $Sr_2Cu_3O_5$) planes[3] made from different arrangements of edge-shared and corner-shared CuO_4 squares. These arrangements are shown in parts a−d Figure 1.

Here we describe a new type of cuprate, $Eu_2CaCu_2O_6$ with CuO_3 planes, prepared by high-pressure synthesis. The structure was determined by combination of exit wave reconstruction and quantitative electron diffraction. The structure contains a new kind of copper oxygen plane, with stoichiometry CuO_3. The plane consists of Cu_2O_6 units composed of two edge-sharing CuO_4 squares, separated from other sets of double squares, and therefore electronically isolated, as shown in Figure 1e. Eu atoms are positioned in a distorted triangular lattice. Measurements of the magnetic properties on this compound reveal dominant antiferromagnetic interactions with an ordering temperature significantly lower than the Curie−Weiss θ, suggesting the presence of geometric magnetic frustration.

Experimental

Polycrystalline $Eu_2CaCu_2O_6$ was prepared as follows. In the first step, Eu_2O_3 (Alfa, 99.99%), CuO (Aldrich, 99.99%), and $CaCO_3$ (Allied Chemical, 99%) were mixed in 1:2:1 molar ratio and heated in air at 850 (12 h), 900 (24 h), and 950 °C (36 h). After the first two heatings the material was ground and pressed into a pellet. The reaction product was examined with powder X-ray diffraction (XRD) and was found to be a mixture of Eu_2CuO_4, $Ca_{1-x}CuO_2$, and CaO. In the second step, the pre-reacted powder was sealed in a gold capsule (5 mm diameter) and pressed in a cubic multi-anvil module in a commercial high-pressure furnace (Rockland Research Corp.). The sample was heated under a pressure of 4.5 GPa, with a heating rate of 50 °C/min, reacted at 850 °C for 4 h, and then quenched under pressure to room temperature.

X-ray powder diffraction data were collected over a range $10 \leq 2\theta \leq 90°$ using a Bruker diffractometer (Cu Kα) equipped with a diffracted-beam monochromator. The diffraction pattern was analyzed with the profile refinement program TOPAS version 2.1 (Bruker AXS).

Electron-transparent areas of the specimens were obtained by crushing them under ethanol to form a suspension and then dripping a droplet of this suspension on a carbon-coated to holey film on a Cu or Au grid. Electron microscopy analysis was performed with a Philips CM300T with an LaB_6 gun for the determination of the

* Corresponding author. E-mail: q.xu@tnw.tudelft.nl. Phone: 31-15-2781201. Fax: 31-15-2786600.
† Delft University of Technology.
‡ Princeton University.
§ Gdansk University of Technology.

(1) Bednorz, J. G.; Müller, K. A. Z *Phys. B* **1986**, *64*, 188.
(2) Cava, R. J. *J. Am. Ceram. Soc.* **2000**, *83*, 5.
(3) Motoyam, N.; Eisaki, H.; Uchida, S. *Phys. Rev. Lett.* **1996**, *76*, 3212.
(4) Weller, M. T.; Lines, D. R. *J. Solid State Chem.* **1989**, *82*, 21.
(5) Azuma, M.; Hiroi, Z.; Takano, M.; Ishida, K.; Kitaoka, Y. *Phys. Rev. Lett.* **1994**, *73*, 3463.
(6) Shaked, H.; Shimakawa, Y.; Hunter. *Phys. Rev. B* **1994**, *50*, 12752.
(7) Rial, C.; Morán, E.; Alario-Franco, M. A.; Amador, U.; Andersen, N. H. *Physica C* **1997**, *288*, 91.
(8) Prado, F.; Caneiro, A.; Serquis, A. *Physica C* **1998**, *295*, 235.
(9) Uzumaki, T.; Kamehara, N.; Niwa, K, *Jpn. J. Appl. Phys.* **1991**, *30*, 981.
(10) Kipka, R.; Hk. Mueller-Buschbaum, Z. *Anorg. Allg. Chem.* **1976**, *419*, 58.

10.1021/cm060725n CCC: $33.50 © 2006 American Chemical Society
Published on Web 08/24/2006

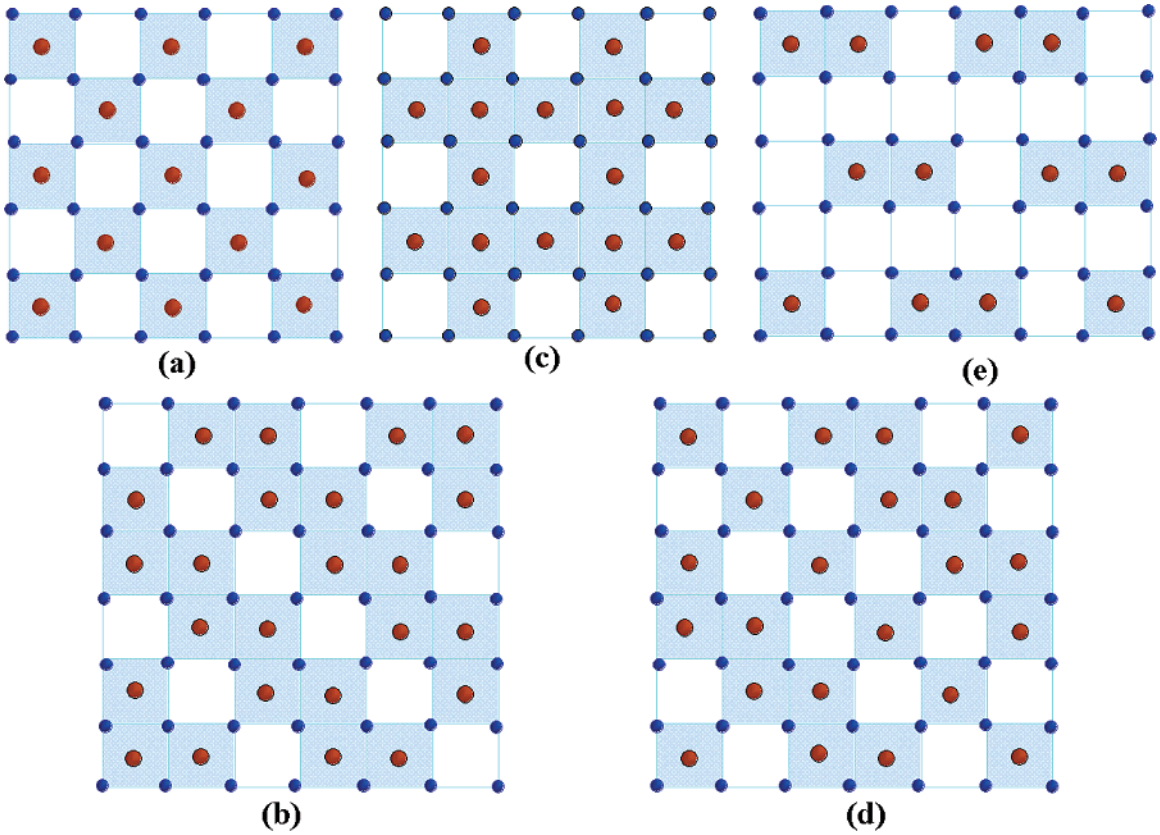

Figure 1. Comparison of the new type of CuO_3 plane found in $Eu_2CaCu_2O_6$ with previously known Cu_xO_y planar arrangements. (a) CuO_2 plane (in HTSC); (b) Cu_2O_3 plane (in $SrCu_2O_3$); (c) Cu_3O_4 (in $BaCu_3O_4Cl_2$); (d) Cu_3O_5 (in $Sr_2Cu_3O_5$); (e) CuO_3 plane (in $Eu_2CaCu_2O_6$). Cu atoms are represented by big light ball balls and O atoms by small red ones.

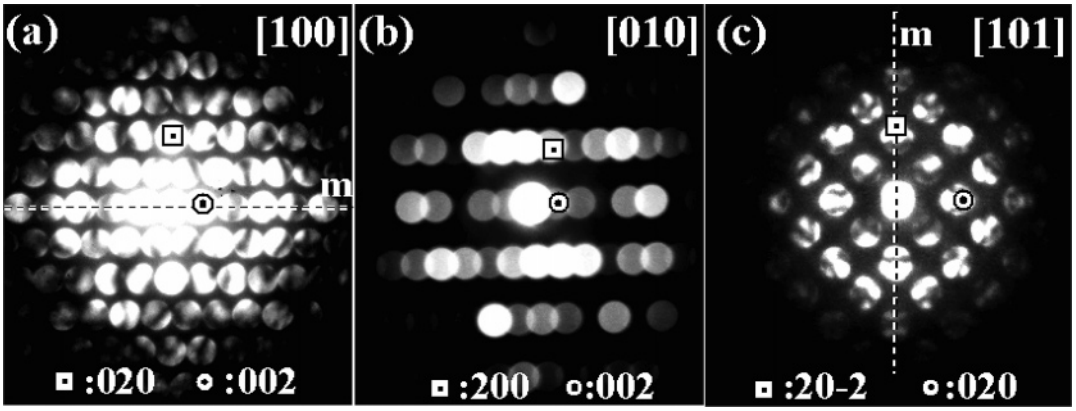

Figure 2. Experimental CBED pattern from $Eu_2CaCu_2O_6$ along three main principal axes. Mirror symmetry can be seen from (a) and (c). The Two-fold axis can be observed from (b).

unit cell and a Philips CM300UT electron microscope having a field emission gun and operated at 300 kV.

The magnetic susceptibility was measured on a powder sample with a SQUID magnetometer (MPMS, Quantum Design) in the temperature range 2−300 K.

Results and Discussion

Structure Determination and Refinement. Unit Cell and Space Group. The initial unit cell parameters were obtained using an electron diffraction tilt series. A good thin single crystal was selected and tilted about a short reciprocal lattice vector, in this case c*. The reciprocal lattice was reconstructed from eight recorded electron diffraction patterns of major zones with tilt range over 90° giving approximate lattice parameters: $a = 6.2$ Å; $b = 6.2$ Å; $c = 15.3$ Å; $\beta = 109°$. Systematic absences were observed for *hkl*: $k + l = 2n$; *h*0*l*: $h,l = 2n$, corresponding to the monoclinic space group $A1a1$ or $A12/a1$. Parts a−c of Figure 2 show the convergent beam electron diffraction (CBED) patterns along the [100], [010], and [101] zone axes. It is clear that a mirror plane perpendicular to the *b* axis and a 2-fold axis along the *b* axis exist, indicating that the space group is $A12/a1$.[11,12] By use of this space group and unit cell, all peaks in the XRD pattern can be indexed (see Figure 3). The unit cell parameters were refined from the X-ray data using the profile refinement program TOPAS version 2.1 (Bruker AXS),

(11) Tanka, M.; Saito, R.; Sekii, H. *Acta Cryst., A* **1983**, *39*, 357.
(12) Yoshio Bando, *Acta Cryst., A* **1982**, *38*, 211.

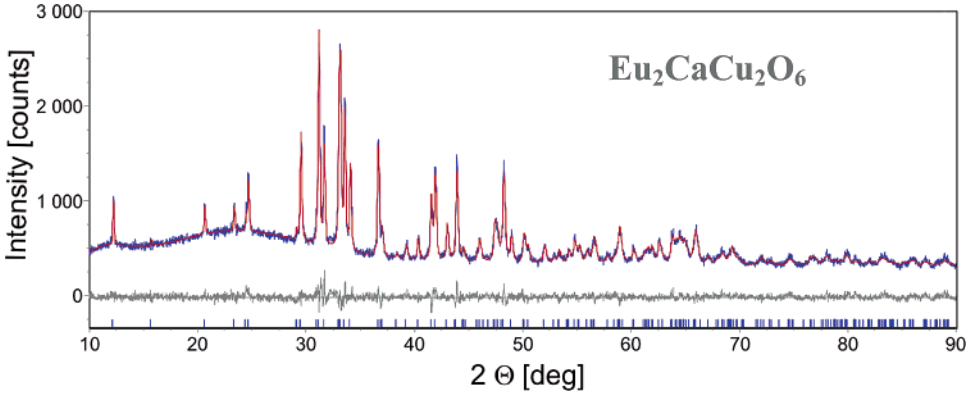

Figure 3. Observed (blue) and calculated (red) powder XRD intensities for $Eu_2CaCu_2O_6$ at 295 K. The difference plot is shown below. Vertical bars at the bottom show the Bragg peak positions.

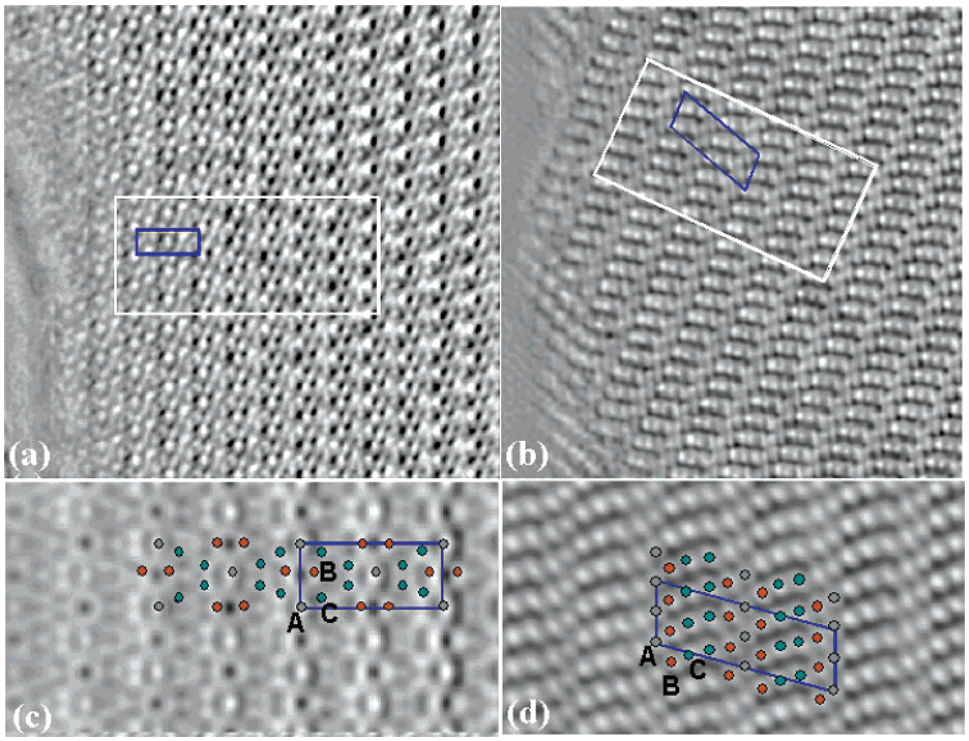

Figure 4. Structure information acquired by HREM. (a) and (b) show the phase of the reconstructed exit wave along [100] and [010] orientation, respectively. The exit wave was reconstructed from a series of 20 experimental HREM images using program Trueimage. (c) and (d) show the part of the exit wave same as in (a) and (b), respectively, but imposed *A*12/*a*1 symmetry by image processing and with an overlay of the atomic positions as deduced from the exit wave. Three unequivalent heavy atom positions A, B, C can be distinguished in (c) and (d).

resulting in $a = 6.084(5)$ Å; $b = 6.148(5)$ Å; $c = 15.34(1)$ Å; $\beta = 108.3(4)°$.

Structure Model. To obtain a starting model for the structure refinement, high-resolution electron microscopy (HREM) was performed. To minimize the distortion caused by microscope optics, the exit wave was reconstructed from a through-focus series of 20 HREM images using Trueimage software.[13−15] In parts a and b of Figure 4, the phase of the reconstructed exit wave along the [100] and [010] zone axes are shown. Since the symmetry of images is frequently lost in high-resolution imaging due to the misorientations of the specimen and residual aberrations, the exit waves were corrected by imposing the known symmetry operations of the *A*12/*a*1 space group onto the images, parts a and b of Figure 4. Parts of the symmetry corrected exit wave along [100] and [010] zone axes are shown with overlays of atomic positions deduced from exit wave in parts c and d of Figure 4, respectively. Three symmetry independent white dots can be observed in the [100] exit wave, suggesting heavy atom positions at A(x_1,0,0), B(x_2,0.5,0.09), and C(x_3,0.82,0.18) (see Figure 4c). Although they have different intensities, assignment of Eu, Cu, and Ca to each of these sites is not possible due to strong dynamical effects in electron diffraction, which results in thickness dependent contrast ratios.[16] On the basis of the interatomic distances between these positions as a function of the *x* coordinate (for instance, by assuming Eu

(13) Zandbergen, H. W.; Andersen, S. J.; Jansen, J. *Science* **1997**, *227*, 1221.
(14) Zandbergen, H. W.; Dyck, D. V. *Microscopy. Res. Tech.* **2000**, *49* 301.
(15) Kübel, C.; Tang, D.; Fliervoet, T.; Thust, A. *Forschungszentrum Jülich, Trueimage Focus Series Reconstruction Package*; FEI Company: 2003.

(16) Van Dyck, D.; Op de Beeck, M. *Ultramicroscopy* **1996**, *64*, 99.

Table 1. Data on the Diffraction Sets Used for the Structure Refinement of $Eu_2CaCu_2O_6$ Listed in Table 2[a]

zone	no. obsd reflns	thickness (nm)[b]	crystal misorientation[b] h	k	l	*R* value (%)
[100]	774	12.7(1)	0	0.8(1)	5.8(1)	7.0
[100]	816	6.9(1)	0	−0.4(1)	4.7(1)	2.6
[100]	1348	6.6(1)	0	1.4(1)	3.0(1)	2.9
[100]	663	9.5(1)	0	0.1(1)	−9.0(1)	3.2
[010]	683	6.8(1)	0.6(1)	0	−0.2(1)	1.1
[011]	426	6.4(1)	0	−1.1(1)	−1.1(1)	1.1
[010]	503	13.0(1)	0.2(1)	0	1.3(1)	2.8
[011]	420	13.5(1)	0	1.4(1)	1.4(1)	3.5
[010]	305	6.1(1)	2.0(1)	0	3.0(1)	2.6
[010]	623	18.9(1)	1.5(1)	0	0.5(1)	4.8
[210]	193	8.2(1)	0.7(1)	−1.5(1)	4.5(1)	1.4
[110]	336	8.5(1)	−0.7(1)	−0.7(1)	−7.8(1)	2.1
[110]	302	8.1(1)	−0.3(1)	−0.3(1)	−8.8(1)	3.4
[100]	446	25.4(1)	0	0.0(1)	0.7(1)	3.4
[100]	517	9.3(1)	0	−0.1(0)	0.0(1)	3.3

[a] The crystal misorientation is given as the position of the projection of the center of the Ewald sphere in Miller indices *h*, *k*, and *l*. [b] For simplicity, only one digit after the decimal was kept for sample thickness and misorientations, resulting in the standard deviations listed above being several orders larger than real. The truncations only induce a 0.02% increase of the *R* value.

at position C and $x_3 = 0.1$, all the interatomic distances between position C(0.1,0.82,0.18) and its other symmetry related positions C′ can be calculated, among which the minimum distance is 2.91 Å, too short for an Eu−Eu distance in an oxide, allowing to conclude that $x = 0.1$ is not good for Eu at positon C), the nominal ratio Eu:Ca:Cu being 2:1:2, the symmetry of these positions, and refinements of several plausible models, a most likely model was constructed with Eu at (0.22,0.82,0.18), Ca at (0.25,0,0), and Cu at (0.5,0.5,0.09), which is also consistent with structure information from symmetry corrected exit wave along [010] axis, shown in Figure 4d. The exit wave of [010] was not used directly to determine the *x* coordinates of the A, B, and C atoms because its interpretation requires a choice of origin compatible to that of the [100] image. Since various choices are possible, we have chosen to make a model based on the [100] exit wave only and use the [010] exit wave as confirmation of the model. Detailed information on the assignment procedure is given elsewhere.[17] Note that a wrong assignment of cations to a certain position in this stage of the structure determination can often be corrected in the more final stage of refinement, since it is more important that the positions are correct than how they are actually occupied. For instance, for a refinement of $Ce_5Cu_{12}P_{19}$ by this method, assuming only Cu on all positions first, and later refining occupancies of these "Cu" sites allowed the successful assignment of Ce, Cu, and P to the various sites and determination of a final structural model.[18]

Structure Refinement. The least-squares refinement package MSLS (multi-slice least squares) was used to refine the structure model acquired above. MSLS takes dynamic diffraction explicitly into account.[18] Oxygen positions were obtained using difference maps. In the final refinement 15 data sets of 4 different zones were simultaneously refined. The overall *R* value after refinement was 3.01%. Table 1 lists the number of reflections, the refined crystal misorientation, and the *R* values of each diffraction pattern. Final structural parameters are given in Table 2. Figure 3 shows that the structural model obtained by electron diffraction yields a good fit to the powder XRD data. The positional coordinates obtained by XRD refinement (see supporting material) are in good agreement with those obtained by electron diffraction. The main differences are in the oxygen positions, which must be due to the relatively poor sensitivity of the powder XRD data to the positions of the oxygen atoms in the presence of heavy cations. Some metal oxygen bond distances obtained by electron diffraction are presented in Table 3.

Table 2. Crystallographic Data for $Eu_2CaCu_2O_6$ from Electron Diffraction[a]

	x	y	z	*B* (Å^2)	occ
Eu	0.21894(5)	0.81157(6)	0.20108(2)	1.598(3)	1
Ca	0.25	0.03447(8)	0	0.055(5)	1
Cu	0.48934(6)	0.59070(8)	0.08228(3)	0.712(5)	1
O1	0.46639(5)	0.48280(3)	0.20189(7)	1.69(2)	1
O2	0.54233(6)	0.88220(2)	0.12383(8)	1.15(2)	1
O3	0.55335(7)	0.30280(3)	0.04345(9)	2.30(3)	1

[a] The unit cell is a = 6.084(5) Å, b = 6.148(5) Å, c = 15.340(2) Å, and $\beta = 108.262(4)°$, and the space group is *A*2/*a*. $R = 3.0\%$.

Table 3. Selected Bond Distances for $Eu_2CaCu_2O_6$

bonds		distance (Å)	bonds		distance (Å)
Eu1−O2	1×	2.30(1)	Cu1−O2	1×	1.90(1)
Eu1−O1	1×	2.38(1)	Cu1−O3	1×	1.95(1)
Eu1−O1	1×	2.38(1)	Cu1−O3	1×	1.98(1)
Eu1−O1	1×	2.39(1)	Cu1−O1	1×	2.00(1)
Eu1−O3	1×	2.41(1)	Ca1−O2	2×	2.35(1)
Eu1−O1	1×	2.52(1)	Ca1−O3	2×	2.41(1)
Eu1−O2	1×	2.63(1)	Ca1−O3	2×	2.58(1)
Eu1−O2	1×	2.88(1)	Ca1−O2	2×	2.64(1)

Description of Structure. The structure of $Eu_2CaCu_2O_6$ consists of CuO_3 planes and Eu_2Ca planes stacked along [100] (see Figure 5a). There are two symmetry-related CuO_3 planes and two symmetry-related Eu_2Ca planes (by a glide mirror plane located at $y = 1/2$) (see parts b−e of Figure 5), such that the staking can be best described as $(CuO_3)_A-(Eu_2Ca)_A-(CuO_3)_B-(Eu_2Ca)_B$, as shown in Figure 5a. The CuO_3 planes are close-packed O planes with Cu atoms forming isolated Cu_2O_6 units (see parts b or d of Figure 5; please note that the O atom radius shown in these two figures are more enlarged than usual to reflect the structure feature of the close packed O anions). The stacking direction [100] is not perpendicular to the stacking planes, resulting in the monoclinic unit cell. To understand the origin of the oblique stacking direction, we can compare a hypothetical structure of $(CuO_3)_A-(Eu_2Ca)_A-(CuO_3)_B$ with an orthorhombic unit cell with the real structure (respectively shown in parts g and f of Figure 5). The eight nearest neighboring O anions around one Eu atom and those around one Ca atom are outlined using dashed lines. In the orthorhombic cell, the eight coordination of Ca is rather symmetric with proper Ca−O distances but that of Eu shows a strong deviation from the ideal one. To optimize the Eu coordination, the $(CuO_3)_B$ plane has to be shifted to the $(CuO_3)_A$ plane resulting in monoclinic distortion. Evidently the amount of monoclinic distortion is a compromise between a better coordination for the Eu atom and the worsened coordination of Ca.

(17) Xu, Q., et al. In preparation.
(18) Jansen, J.; Tang, D.; Zandbergen, H. W.; Schenk, H. *Acta Cryst., A* **1998**, *54*, 91.

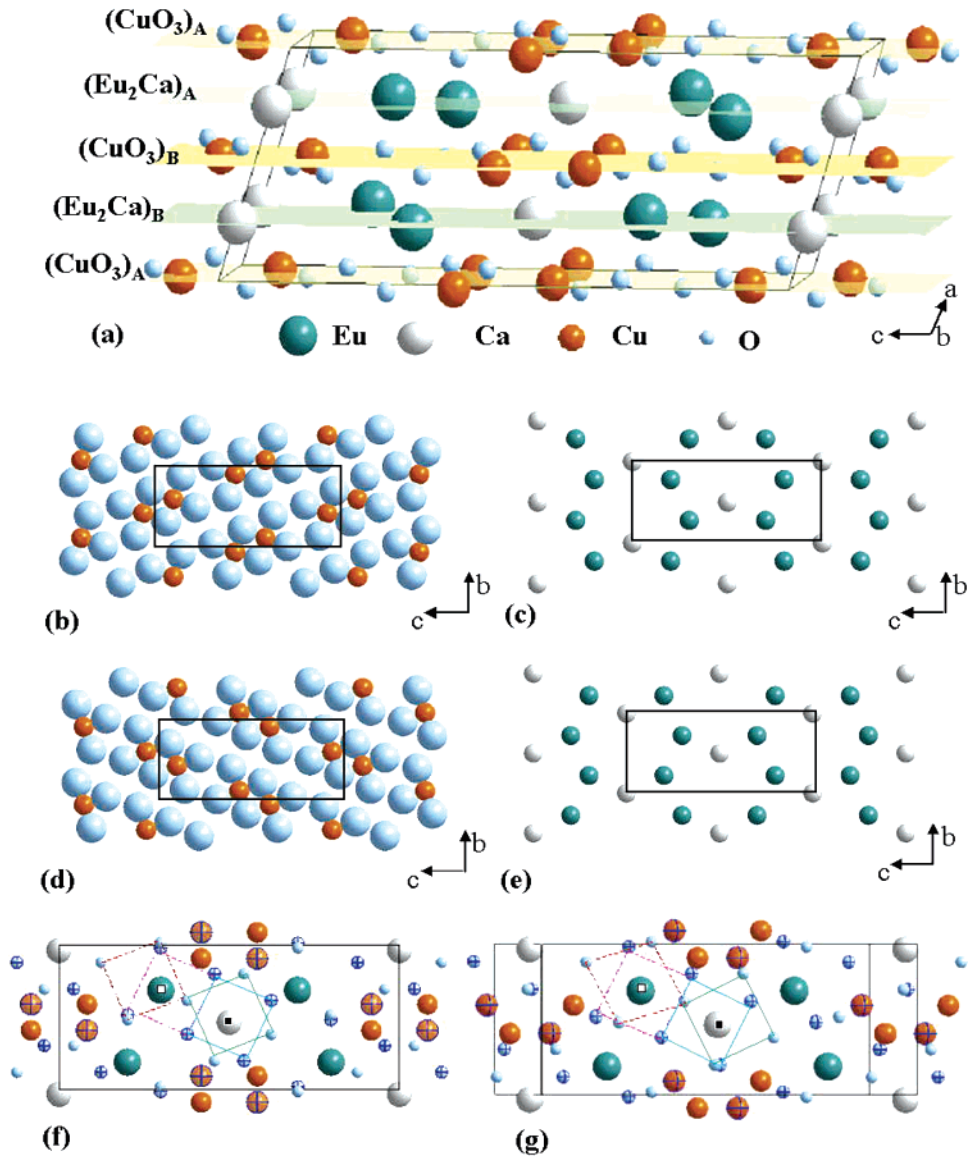

Figure 5. Schematic representation of the structure of $Eu_2CaCu_2O_6$ (a) as a whole displaying the different layers, (b)−(e) showing the different layers, and (f−g) showing the reason for the monoclinic distortion. (a) The four type of planes stacking in the order $(CuO_3)_A-(Eu_2Ca)_A-(CuO_3)_B-(Eu_2Ca)_B$ are indicated, which are given as separated layers in (b)−(e) (looking this time perpendicular to the layers. (To reflect the structure feature of the close packed O anions, the O atom radius shown in parts b and d of Figure 5 are enlarged than usual.) (f) shows a Eu_2Ca plane with two neighboring CuO_3 planes for the hypothetic structure without monoclinic distortion. (g) shows the same planes but with the real monoclinic distortion. The oxygen environment of Eu and Ca are both indicated by colored dashed lines in (f) and (g) It can be noted that without monoclinic distortion, Ca atom is at the exact center of its eight nearest neighboring O atoms but Eu atom is not at all, which is higly unfavorable. By applying a monoclinic distortion, Eu atom move to a more stable position at expense Ca are not at exact center of eight neighboring O atoms.

From Figure 5b, we can also clearly see that Cu_2O_6 units are isolated, giving this cuprate a zero-dimensional structural character. These Cu_2O_6 units are composed of two edge-sharing CuO_4 units with Cu−O bond length in the range of 1.90 and 2.00 Å, close to the typical Cu−O bond lengths found, e.g., 1.95 Å in Eu_2CuO_4[19] and 1.96 and 1.97 Å in Sr_2CuO_3.[20] In one Cu_2O_6 unit, two Cu atoms and two sharing O atoms form a Cu_2O_2 square with Cu−O bond length of about 1.96 Å. The other four Cu−O bonds are twisted away from the Cu_2O_2 square plane (11.8 and 20.8°, respectively), possibly due to the influence of Eu−O bonding. These features are displayed in polyhedral style in parts a and b of Figure 6. From Figure 6c, we can see that these Cu_2O_2 squares are not exactly in the common plane (100) but tilted up to 13.5° away from the plane instead. Note that apart from the four "normal" Cu−O bonds the Cu atoms have other O atoms at 2.61 and 2.94 Å, respectively, which should not be considered as bonding distances.

The Eu and Ca atoms are bonded to eight oxygen atoms in the ranges of 2.30−2.88 Å and 2.35−2.64 Å, respectively. Those oxygen atoms form a distorted square antiprism. (See parts d and e of Figure 6). Note that each Eu_2Ca layer is composed of zigzag Eu chains and straight Ca chains (see Figure 5c). By stacking Eu_2Ca layers along [100] direction, those zigzag Eu chains will build up a series of double Eu sheets, which contain all the nearest Eu−Eu distances.

(19) Uzumaki, T.; Hashimoto, K.; Kamehara, N. *Physica C* **1992**, *202*, 175.
(20) Lines, D. R.; Weller, M. T.; Currie, D. B.; Ogborne, D. M. *Mater. Res. Bull.* **1991**, *26*, 323.

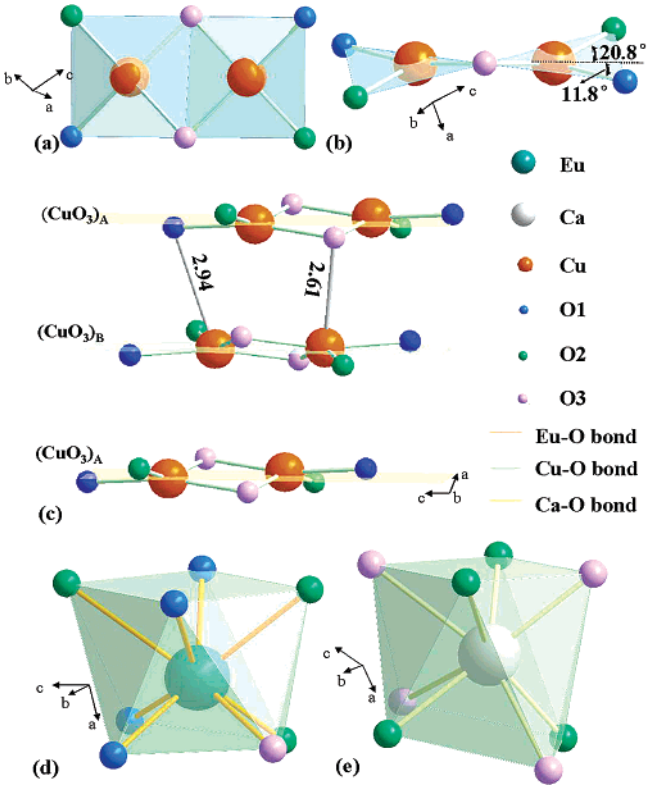

Figure 6. (a), (b), and (c−e) give the coordination environments of Cu−O, Eu−O, and Ca−O, respectively. Note that Cu−O "bonds" between Cu and two types of apical O atoms are represented by different color sticks with "bond" length noted.

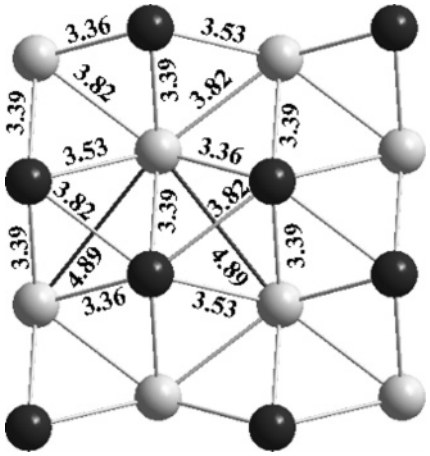

Figure 7. The Eu network with nearest Eu−Eu distance noted. Eu atoms on different *ab* planes are represented by different gray balls.

Eu is the dominant magnetic ion in the compound. Magnetic interactions between Eu atoms are via direct exchange. Thus, for understanding these interactions it is important to describe the Eu−Eu network. One double Eu sheet with nearest Eu−Eu distances labeled is shown in Figure 7, where Eu atoms on different *ab* planes are depicted as different gray spheres. From Figure 7 we can see that each Eu atom neighbors eight Eu atoms, four on the same *ab* plane and four on different *ab* planes via corner, edge and face sharing of Eu−O polyhedra. Different connections of the Eu−O polyhedra result in different Eu−Eu distances. Sharing a square face or a triangle face of the Eu−O square antiprisms gives the smallest Eu−Eu distances: 3.36 or 3.39 Å, respectively; sharing square edges or triangle edges gives

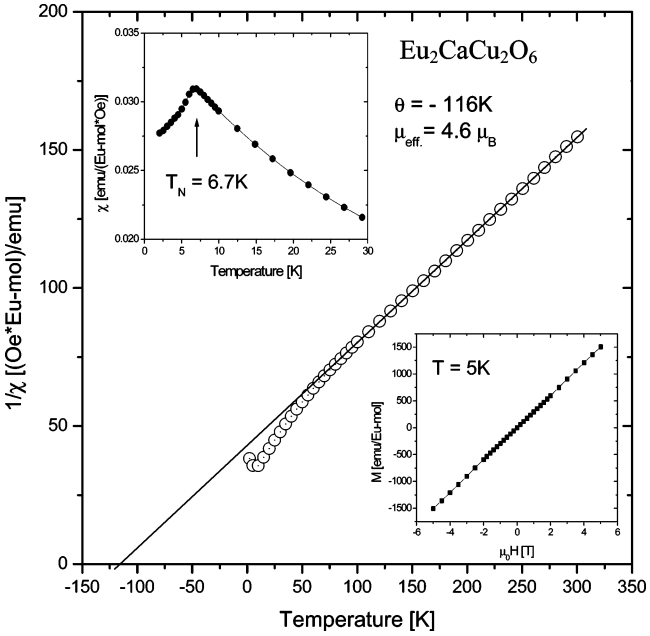

Figure 8. Inverse of magnetic susceptibility ($1/\chi$) vs T of $Eu_2CaCu_2O_6$. The line represents the Curie−Weiss fit. Top inset: temperature variation of the magnetic susceptibility (χ). Bottom inset: magnetization (M) vs magnetic field (μ_0H) at $T = 5$ K.

Eu−Eu distances of 3.53 or 3.82 Å; and finally, sharing corners gives the largest distance, 4.89 Å. This latter distance is not likely to be important in the magnetic interactions to first order, and thus, as shown in the figure, the Eu array is best simply described as a simple puckered triangular lattice.

The similarity between the coordination of Eu atoms and the coordination of Ca atoms (see parts d and e of Figure 6) implies that Eu and Ca atoms might be substituted for each other. We observed this type of substitution in crystals with a composition $(Eu_{0.5}Ca_{0.5})_2CaCu_2O_6$ obtained in a reaction mixture with nominal composition $Eu_2Ca_2Cu_3O_8$. The crystals $(Eu_{0.5}Ca_{0.5})_2CaCu_2O_6$ have the same crystal structure as $Eu_2CaCu_2O_6$ but with the Eu sites now half substituted by Ca atoms. The crystallographic data for $(Eu_{0.5}Ca_{0.5})_2CaCu_2O_6$ are given in the Supporting Information.

Magnetic Properties. The zero-field cooled DC magnetization data for $Eu_2CaCu_2O_6$, measured on heating under an applied magnetic field of 1 T, are presented in Figure 8. The figure shows the inverse of magnetic susceptibility between 2 and 300 K. The high-temperature part (above 75 K) is well described by a Curie−Weiss law with net effective antiferromagnetic coupling $\theta = -116$ K and effective magnetic moment of $\mu_{eff} = 4.6\ \mu_B$/mol Eu ($\mu_{eff} = 6.5\ \mu_B$/mol $Eu_2CaCu_2O_6$). The substantial deviation from the Curie−Weiss law for temperatures below 70 K might suggest the appearance of ferromagnetic fluctuations in this temperature range. However magnetic moment vs magnetic field measurements at 5 K (see inset) show linear behavior, indicating that no ferromagnetism is observed at 5 K. The magnetic moment displayed by Eu^{3+} is generally near 3.4 μ_B/mol Eu,[21] which is much lower than the experimental effective magnetic moment of $\mu_{eff} = 4.6\ \mu_B$/mol Eu. Thus it can be concluded that Cu^{2+} also contributes to the effective magnetic

(21) Kittel, C. *Introduction of Solid State Physics*, 6th ed.; Wiley: New York, 1986.

moment. However, due to strong crystal field effect, as in the related compound Eu_2CuO_4,[22] the total effective moment for $Eu_2CaCu_2O_6$ derived from Curie−Weiss fits could not be simply interpreted as arising from the sum of the ideal contributions of Eu^{3+} and Cu^{2+}.

The top inset of Figure 8 shows χ vs T in the low-temperature range. A magnetic ordering transition is observed at $T_N = 6.7$ K. The transition may be due to either Cu^{2+} or Eu^{3+} ordering independently, or alternatively both magnetic systems may order at the same temperature. There is no indication of a dimerlike contribution to the susceptibility from the Cu−O lattice despite its geometry. Such a contribution would consist of a broad peak in $\chi(T)$ with a maximum at a temperature related to the strength of the magnetic coupling. The very large magnetic contribution of the Eu would obscure the contribution of the Cu dimer susceptibility even if present. Attempts to synthesize this compound with the nonmagnetic rare Y were not successful, and therefore the behavior of the Cu dimers cannot be determined from static susceptibility measurements. Another interesting point should be noted that the ratio of the observed θ and T_N is 17, and we therefore tentatively conclude that $Eu_2CaCu_2O_6$ is an example of a strongly frustrated material.[22,23] The origin of the frustration is likely found in the edge-shared triangle geometry of the Eu lattice. The complexities of this material from a magnetic standpoint suggest that further study may be of interest.

(22) Tovar, M.; Rao, D.; Barnett, J.; Oseroff, S. B.; Thompson, J. D.; Cheong, S.-W.; Fisk, Z.; Vier, D. C.; Shultz, S. *Phys. Rev. B* **1989**, *39*, 2661.
(23) Ramirez, A. P. *Annu. Rev. Mater. Sci.* **1994**, *24*, 453.

Summary and Conclusions

Polycrystalline $Eu_2CaCu_2O_6$ was synthesized at high pressure. The structure of $Eu_2CaCu_2O_6$ was solved by the combination of exit wave reconstruction and quantitative electron diffraction refinement and confirmed by X-ray Rietveld analysis. The structure contains CuO_3 planes, which are built up by separated Cu_2O_6 units. Compared with the CuO_2 plane in HTSC cuprates, CuO_3 plane can be characterized by a different manner of filling Cu^{2+} ions into the interstitial position of O^{2-} anions. Eu atoms are found in a puckered triangular planar lattice having distorted square antiprism coordination. Magnetic measurements indicate antiferromagnetic behavior with magnetic frustration. It will be of interest to determine whether other materials with related structure types can be found.

Acknowledgment. The work at Delft was supported by The Nederlandse Stichting voor Fundamenteel Onderzoek der Materie. The research at Princeton was supported by the US Department of Energy, Basic Energy Sciences, Grant DE FG02-98-ER45706. T.K. acknowledges support from the Foundation for Polish Science.

Supporting Information Available: Tables of crystallographic information, data on diffraction sets, and selected bond distances (PDF) as well as crystallographic information files in CIF format. This material is available free of charge via the Internet at http://pubs.acs.org.

CM060725N